Progress In Electromagnetics Research M, Vol. 22, 219–232, 2012

ROBUST TECHNIQUES FOR COHERENT CHANGE DETECTION USING COSMO-SKYMED SAR IMAGES

A. Bouaraba[1,*], A. Younsi[1], A. Belhadj-Aissa[2], M. Acheroy[3], N. Milisavljevic[3], and D. Closson[3]

[1]Ecole Militaire Polytechnique, Bordj el Bahri, BP 17, Algiers, Algeria

[2]University of Sciences and Technology Houari Boumedienne, El Alia, BP 32, Bab Ezzouar, Algiers, Algeria

[3]Royal Military Academy, Avenue de la Renaissance 30, 1000 Brussels, Belgium

Abstract—The satellite-borne SAR (Synthetic Aperture Radar) is a quite promising tool for high-resolution geo-surface measurement. Recently, there has been a great interest in Coherent Change Detection (CCD), where the coherence between two SAR images is evaluated and analyzed to detect surface changes. The sample coherence threshold may be used to distinguish between the changed and unchanged regions in the scene. Using COSMO-SkyMed (CSK) images, we show that for changed areas, the coherence is low but not completely lost. This situation, which is caused by the presence of bias in the coherence estimate, considerably degrades the performance of the sample threshold method. To overcome this problem, robust detection in inhomogeneous data must be considered.

In this work, we propose the application and improvement of three techniques: Mean Level Detector (MLD), Ordered Statistic (OS) and Censored Mean Level Detector (CMLD), all applied to coherence in order to detect surface changes. The probabilities of detection and false alarm are estimated experimentally using high-resolution CSK images. We show that the proposed method, CMLD with incorporation of guard cells (GC) in the range direction, is robust and allows for nearly 4% higher detection probability in case of low false alarm probability.

Received 7 November 2011, Accepted 16 December 2011, Scheduled 22 December 2011

* Corresponding author: Azzedine Bouaraba (abouaraba@gmail.com).

1. INTRODUCTION

Remote sensing is one of the most important technologies for monitoring changes occurring on the Earth surface (e.g., land cover change analysis, nature disaster estimation). Compared to optical remote sensing, SAR sensors present the advantage of being independent of atmospheric and sunlight conditions. From this point of view, SAR data offer a great potential for monitoring applications in cloudy or rainy regions [1]. Change detection with remote sensing SAR images involves a pair of co-registered images acquired over the same area at different times. To identify changes, different methods are commonly applied. These methods differ with respect to the parameter that is used to indicate changes and to the technique that is used to reduce the noise. Since SAR data contain amplitude and phase information, both parameters can be used as change indicators [2]. Two forms of change detection in repeat-pass SAR imagery may be considered, namely coherent and incoherent change detection [3]. Incoherent change detection identifies changes in the mean backscatter power of the scene by comparing sample estimates of the mean backscatter power taken from the repeat pass image pair. Typically, sample estimates are obtained by averaging spatially the image pixel intensities over local regions in the image pair [4]. Coherent change detection, on the other hand, uses the magnitude of the sample complex cross correlation of an interferometric SAR image pair to quantify changes in the observed amplitude and phase of the image pixels. In [5], the accuracy of coherence estimation was investigated as a function of the coherence map resolution. It has been demonstrated that the sample coherence magnitude estimator is biased especially for low coherence values. Also, it is shown that the averaged sample coherence permits the calculation of an unbiased coherence estimate over a sufficiently coarse resolution cell. An improved change detection is presented in [3]. Here, models describing the changed and unchanged regions of a scene are postulated and the detection performance of a new log-likelihood change statistic is demonstrated using experimental data. The sensitivity of the scene coherence in detecting subtle scene changes has been demonstrated in [6], where low-coherence tracks, possibly due to scene disturbances arising from grazing sheep, were detected. Recently, there has been a great interest in Coherent Change Detection. In [7], a new method has been presented to improve the coherence between SAR images for coherent change detection by removing the fringe rate, which is determined by the terrain topography and the interferometric baseline. This technique can clarify the low coherence area due to the terrain change

by improving coherence in the unchanged area. In [8], an analytic framework for systematic coherent change detection is established by taking advantage of the analytical relation to partially polarized electromagnetic fields. It is shown by analytic reasoning and through examples that the degree of coherency and excess coherency factor can be used to enhance change characterization. In [9], a novel detection index for CCD of the complex SAR images has been proposed. The experimental investigation proved that the proposed method provides almost 10% higher detection probability compared to the coherence method. In [3, 6], the authors make the assumption that for X-band radars, man-made disturbances can potentially cause significant scatterer displacement, and hence a complete loss in coherence. In the present work, we verify experimentally by processing six CSK images with different time interval, that for all changed areas (caused by agricultural activities), the coherence is low but not completely lost. This situation, which is caused by the presence of bias in the coherence estimate especially for low values [5], degrades considerably the detection performance of the sample threshold detector (see Section 5).

In the present paper, we propose an improvement to three techniques that are applied to coherence in order to detect surface changes. The probabilities of detection and false alarm are estimated experimentally using high-resolution CSK images. This type of data is characterized by some samples of high coherence in the changed area (inhomogeneous data). These samples are considered as outliers and must be discarded. The detector, which takes into account this issue, is commonly called "robust detector" in the sense that its performance is unchanged or at least slightly affected by the presence of outliers. We show that the use of the CMLD may enhance the detection performance and particularly if we add guard cells in the range direction.

This paper is organized as follows. In Section 2, the interferometric coherence is presented. It is shown that interferometric coherence can be expressed as a product of a number of dominant contributions and reflects the true scene disturbance. Section 3 concerns the MLD, OS and CMLD detectors. Section 4 deals with the proposed method which is based on the incorporation of GC. Section 5 is devoted to the application of the presented detectors using experimental data. The conclusion is given in the final section.

2. INTERFEROMETRIC SAR COHERENCE

In order to provide some measure of discrimination in the image pair and accommodate the random noise fluctuations, the degree of similarity between the image pair is quantified by the sample coherence. The sample coherence is defined as the magnitude of the sample complex cross correlation coefficient between the image pair [1, 2]:

$$\gamma = \frac{\left|\sum_{i=l}^{N} f_i g_i^*\right|}{\sqrt{\sum_{i=l}^{N} |f_i|^2 \sum_{i=1}^{N} |g_i|^2}} \tag{1}$$

Here, the sample cross correlation coefficient measures the average correlation between images f and g over an N-pixel local area in the scene and encodes the degree of scene similarity as a value in the range $[0, 1]$. The coherence may be expressed as the product of a number of dominant contributions [6]:

$$\gamma = \gamma_{\text{SNR}}\gamma_{\text{base}}\gamma_{\text{scene}}\gamma_{\text{vol}}\gamma_{\text{proc}} \tag{2}$$

The component γ_{SNR} is determined by the relative backscatter signal to radar receiver noise ratio in the interferometric image pair [2, 10]. γ_{base} quantifies the decorrelation that arises due to mismatch in the acquisition geometries in the primary and repeat-pass collections [11]. γ_{vol} quantifies the decorrelation that arises when the images are acquired with a nonzero baseline and the scattering occurs from a volume such as a vegetated area [10, 12]. The decorrelation depends on the properties of the scattering volume such as the extinction coefficient, as well as the interferometric baseline and the polarization of the incident radiation [3]. The processing can eliminate γ_{vol} only in case of zero normal baseline which is never achieved for spaceborne sensors. The component γ_{proc} quantifies the decorrelation arising from mismatch between the coherent acquisition apertures and image-formation processing stages used to produce the primary and repeat-pass imagery. The coherence term γ_{scene} quantifies the decorrelation in the scene over the repeat-pass time interval, e.g., man-made scene disturbances [3]. Through a careful design of the repeat-pass imaging geometry and appropriate interferometric processing steps, it is possible to achieve $\gamma_{\text{SNR}}\gamma_{\text{base}}\gamma_{\text{proc}} \simeq 1$ [3]. In this case, the coherence γ of the scene image will reflect the underlying true scene coherence γ_{scene}.

3. DETECTION METHODS

3.1. Mean Level Detector (MLD)

A simple threshold applied to the coherence may be used to distinguish between the changed and unchanged regions in the scene. This detector offers low detection performance, see Section 5. In order to improve the performance, one can evaluate the mean of sample coherence over an M-pixel local area. This method, developed in [5], was proposed as a bias removal of coherence estimate:

$$z_1 = \frac{1}{M}\sum_{i=1}^{M}\gamma_i \underset{H_1}{\overset{H_0}{\gtrless}} T_1 \tag{3}$$

where H_0 is a realization of the null hypothesis (scene changes of interest absent) and H_1 is the alternative hypothesis (scene changes of interest present). To make a decision, the statistic z_1 is compared to a threshold T_1.

3.2. Ordered Statistic Coherence Detector (OS)

The ordered statistic detector [13] was initially proposed to deal with impulsive interference. It can be used to detect changes by evaluating the following statistic:

$$z_2 = \gamma'_{n_{os}} \underset{H_1}{\overset{H_0}{\gtrless}} T_2 \tag{4}$$

where $\gamma'_1 \leq \gamma'_2 \ldots \leq \gamma'_M$ are the ordered sample coherence values over an M-pixel local area and n_{os} is the order of the selected sample. In order to make a decision, the statistic z_2 is compared to a threshold T_2. Note that the order n_{os} determines the detection performance of the statistic z_2.

3.3. Censored Mean Level Detector (CMLD)

The CMLD detector is based on the combination of the two statistics z_1 and z_2 [14]:

$$z_3 = \frac{1}{k}\sum_{i=1}^{k}\gamma'_i \underset{H_1}{\overset{H_0}{\gtrless}} T_3 \tag{5}$$

where $k \in [1,\ M]$ is the length of selected and ordered sample coherence over an M-pixel local area. The statistic z_3 is compared to a threshold T_3 to decide if the pixel under test is made from hypothesis H_0 or H_1. Note that for $k = M$, z_3 is identical to the statistic z_1.

4. PROPOSED METHOD

In the present work, we study the spatial correlation coefficient for the coherence obtained by CSK data. We find that for a one pixel shift, the correlation is about 0.4 in the azimuthal direction and 0.8 in the range direction.

In order to keep more details in the changed scene, our proposed methods are based on the incorporation of guard cells (GC) only in the range direction. The evaluation of such statistics z_1, z_2 and z_3 with using of GC means that the two pixels (cells) directly adjacent to the pixel under test have been ignored (see Fig. 1(b)). In radar detection procedures, GC is mostly used to enhance clutter power estimation [13].

5. APPLICATION TO EXPERIMENTAL DATA

To investigate the detection performance of the proposed method, a repeat-pass interferometric process is achieved with CSK images. The acquired SAR data are in X-band, horizontally polarized, with azimuth resolution of 0.71 m, and a range resolution of 0.60 m in spotlight mode. The incident angle is 41.5°. The coregistration of the SAR images was performed by using Sarscape software (© Sarmap 2011). Our programs were developed in IDL (Interactive Data Language). The characteristics of the used data are summarized in the Table 1. The

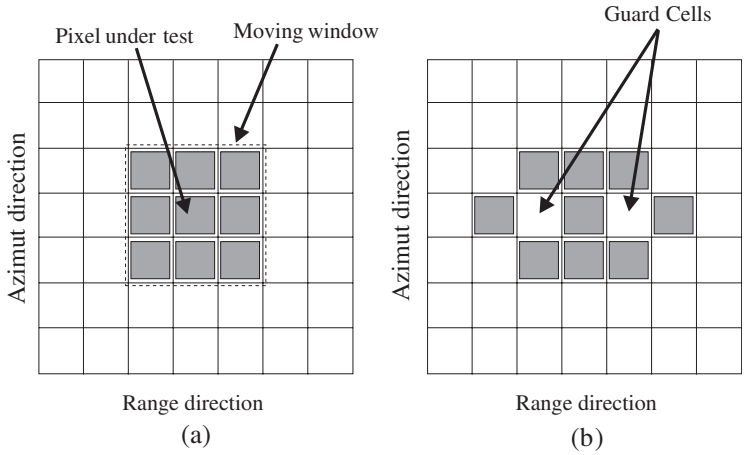

Figure 1. Moving window configurations. (a) Classical moving window. (b) Moving window with incorporation, in range direction, of two guard cells directly adjacent to the pixel under test.

Table 1. CSK SAR images characteristics.

Image N°	Date	Time	Incident angle	Format
01	January 01, 2010	01 : 47 : 28	41.5°	SCS-B
02	January 09, 2010	01 : 47 : 22	41.5°	SCS-B
03	January 10, 2010	01 : 47 : 19	41.5°	SCS-B

Figure 2. Optical image from Google Earth of the studied area. The red rectangle indicates the area of interest corresponding to the SAR image sub-chip size of 750×750 pixels.

area of interest is situated several hundred meters west of Maimana airport, Afghanistan.

The geographical location is shown in Fig. 2 and we can distinguish quite clearly the agricultural parcels. Fig. 3 shows the pair of SAR images (sub-chip size of 750×750 pixels) acquired on January 09 and January 10, 2010. The scene mainly consists of agricultural fields and the two SAR images would appear identical to the eye.

Figure 4 depicts the sample coherence map obtained from the image pair using a 3×3 sliding estimation window. Light-colored pixels represent values of γ near 1, while dark pixels represent values near 0. The map shows three changed areas corresponding to cultivated parcels with low values of coherence. Coherence subsets have been geocoded and then projected in Google Earth to perform a comparison with high-resolution optical images (see Fig. 2). Fig. 5 shows histograms of the selected changed, unchanged and the full scene coherence values. For the unchanged area, the coherence is higher and corresponds to

the coherence of the total scene. This indicates that the selected area faithfully represents the unchanged scene. For the selected changed area, the histogram of coherence indicates unfortunately many pixels with high values of coherence and the mean value of coherence is about 0.43. Note that the authors in [3, 6] make the assumption that for X-band radars, man-made disturbances can potentially cause significant scatterer displacement, and hence a complete loss in coherence. The

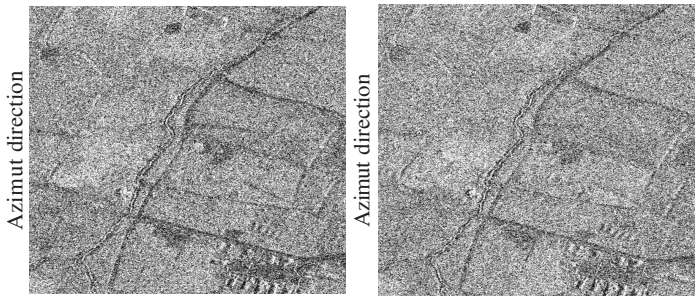

Figure 3. COSMO-SkyMed SAR images. (a) Acquisition of January 09, 2010. (b) Acquisition of January 10, 2010. *COSMO – SkyMed*^{TM} *Product* — ASI [2010] processed under license from ASI — Agenzia Spaziale Italiana. All rights reserved.

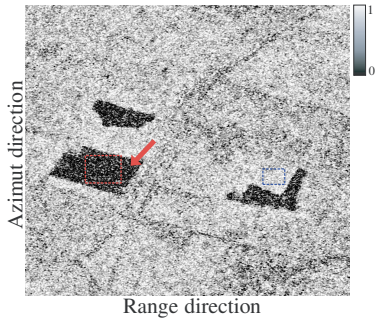

Figure 4. Sample coherence evaluated over the repeat-pass image pair using 3×3 pixel spatial estimation window. Light-colored pixels represent values of coherence near 1, while dark pixels represent values near 0. The arrow indicates one cultivated parcel with low value of coherence. The red rectangle shows the selected changed area and the blue rectangle shows the selected unchanged area.

data used in the present work (six CSK images) demonstrate that for all area changed caused by agricultural activities, the coherence is low but not completely lost. This may be explained by the fact that the sample coherence estimator is biased, especially for low coherence values [5]. In that situation, detection in the presence of inhomogeneous data must be considered. The detectors based on the ordered statistic (OS and CMLD) aim at overcoming this difficulty by rejecting some samples with high coherence value over an M-pixel local area. The simple threshold applied to the different statistics (z_1, z_2 and z_3) may be used to distinguish between the changed and unchanged regions in the scene. For a given threshold T, the detection performance may be quantified by evaluating the probability of detection P_d and the corresponding

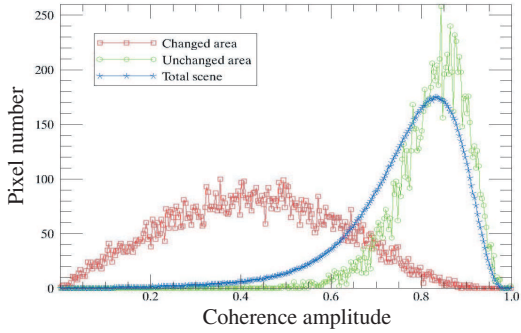

Figure 5. Histograms of the selected changed, unchanged and the total scene coherences.

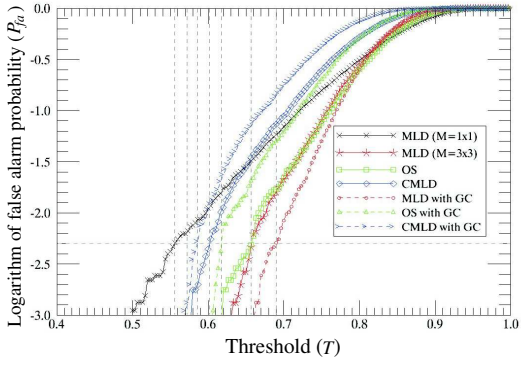

Figure 6. Experimental probability of false alarm versus threshold T. $M = 3 \times 3$, $n_{os} = 5$ and $k = 5$.

probability of false alarm P_{fa} [3]:

$$P_d = \int_0^T P(\hat{\gamma}|\gamma = \gamma_{changed})d\hat{\gamma} \tag{6}$$

$$P_{fa} = \int_0^T P(\hat{\gamma}|\gamma = \gamma_{unchanged})d\hat{\gamma} \tag{7}$$

Now we consider the detection performance of the detectors presented above. The procedure used to estimate experimentally P_{fa} and P_d is based on Equations (6) and (7). At first, the selection of the changed and unchanged areas must be done carefully. The selected changed area (inside cultivated parcel in Fig. 4 is composed of N_c pixels and the selected unchanged area (blue rectangle in Fig. 4 is composed of N_u pixels. The pixel under test is set in the middle of the moving window which is sliding to scan all coherence data of the selected changed area. To evaluate the actual probability of detection, we perform the test given by Equation (3), (4) or (5). The actual P_d is then given by the ratio of the total number of times the test exceeds the threshold and the total number data in the selected changed area (N_c). Similarly, the probability of false alarm can be evaluated by using coherence data of the selected unchanged area. The actual P_{fa} is then given by the ratio of the total number of times the test exceeds the threshold and the total number data in the selected unchanged area (N_u). In the present work, $N_c = 110 \times 115$ and $N_u = 61 \times 40$. Fig. 6 shows the probability of false alarm versus threshold T plots obtained for several detectors. For a given P_{fa} value, e.g., $P_{fa} = 5 \times 10^{-3}$ (see the horizontal line), each detector requires distinct threshold value T_i to offer a probability of detection P_d. Fig. 7(a) shows the results obtained by the mean sample coherence change statistic with $M = 1 \times 1$ (this corresponds to the case of a simple threshold operation with $T = 0.556$). This detector provides $P_d = 0.734$. When increasing the number of pixels M in the local area and for the same P_{fa}, the probability of detection increases. This is presented in Fig. 7(b) with $M = 3 \times 3$ and $T = 0.656$. In this case the MLD gives $P_d = 0.958$. The increase of the probability of detection from Figs. 7(a) to 7(b) is clearly noticeable. These results match those obtained in [5], that the spatial averaging of coherence samples improves the estimation of coherence, especially of low values. Fig. 7(c) shows the CMLD change map obtained with the following parameter values: $M = 3 \times 3$, $k = 5$ and $T = 0.603$. This detector provides $P_d = 0.968$, which is a value larger than for the MLD and OS detectors. Hence, CMLD offers the best performance.

Figure 7(d) shows the change map obtained with CMLD using two guard cells in the range direction and the following parameter values:

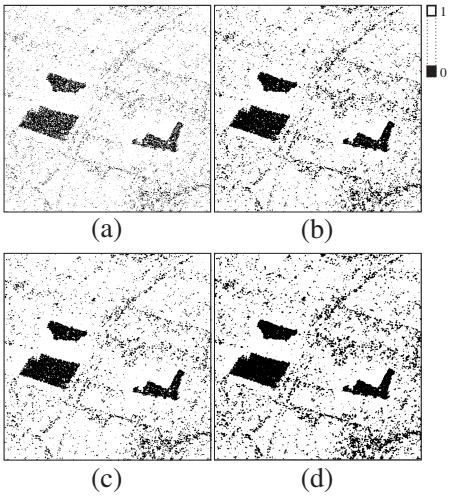

Figure 7. Change detection results for $P_{fa} = 5 \times 10^{-3}$. (a) MLD change map with $M = 1 \times 1$, $T = 0.556$, and $P_d = 0.734$. (b) MLD change map with $M = 3 \times 3$, $T = 0.656$, and $P_d = 0.958$. (c) CMLD change map with $M = 3 \times 3$, $T = 0.603$, $k = 5$, and $P_d = 0.968$. (d) CMLD (with GC)change map for $M = 3 \times 3$, $T = 0.587$, $k = 5$, and $P_d = 0.994$.

$M = 3 \times 3$, $k = 5$ and $T = 0.587$. A comparison with Fig. 7(c) shows a significant enhancement in the detection process. This is achieved at expense of a loss of resolution in the corresponding detected changed scene. The detection performance and the parameter values of the studied detectors are summarized in Table 2. CMLD gives the highest probability of detection for $P_{fa} = 5 \times 10^{-3}$. The detection performance of the proposed method may be improved by increasing the estimation-window size M. However,the window size must be commensurate with the size of the scene disturbances to be detected. We have verified that CMLD performs better than MLD and OS even after an increase of M.

In order to assess the validity of the proposed detectors, the detection performance is evaluated by computing the associated ROC (Receiver Operating Characteristic) curves, which indicate, for a given detection threshold T, the probability P_d of detecting a changed pixel and the corresponding probability P_{fa} of false alarm. The experimental detection performance is shown in Fig. 8 and indicates that CMLD outperforms both MLD and OS. This improvement in the probability of detection is significant for low probability of false alarm ($P_{fa} < 10^{-2}$). For high false alarm rates ($10^{-2} < P_{fa} < 1$), CMLD performs as good

Table 2. Thresholds and corresponding probability of detection Pd. $P_{fa} = 5 \times 10^{-3}$ and $M = 3 \times 3$.

Detectors	Threshold (T)	P_d
MLD ($M = 1 \times 1$)	0.556	0.734
MLD ($M = 3 \times 3$)	0.656	0.958
OS ($n_{os} = 5$)	0.656	0.937
CMLD ($k = 5$)	0.603	0.968
MLD with GC	0.690	0.992
OS with GC ($n_{os} = 5$)	0.617	0.985
CMLD with GC ($k = 5$)	0.587	0.994

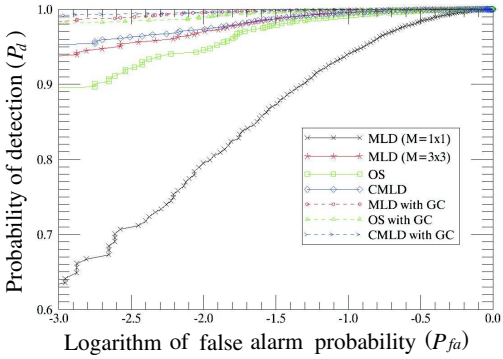

Figure 8. Experimental ROC curves corresponding to the acquisitions of January 09 and January 10, 2009. $M = 3 \times 3$, $n_{os} = 5$ and $k = 5$.

as MLD and OS. These results show that the proposed detectors, which are based on the incorporation of GC in the range direction, allow for an increase of nearly 4% in detection probability at $P_{fa} < 10^{-3}$.

Figure 9 shows the detection performance obtained by the acquisitions of January 01 and January 09, 2009. In this situation, the mean value of coherence in the changed area is about 0.52. Compared to Fig. 8, the detection of changes is more difficult because of the presence of lot of pixels with high value of coherence inside the changed area. The performance of the MLD, OS and CMLD detectors is significantly degraded. We can see also that the incorporation of GC leads to an improvement of detection especially for the CMLD with GC which allows the best performances. The detection performances, as shown in Fig. 8 and Fig. 9, demonstrate that the proposed detector (CMLD with GC) is robust with respect to the presence of pixels with high coherence inside of the changed area.

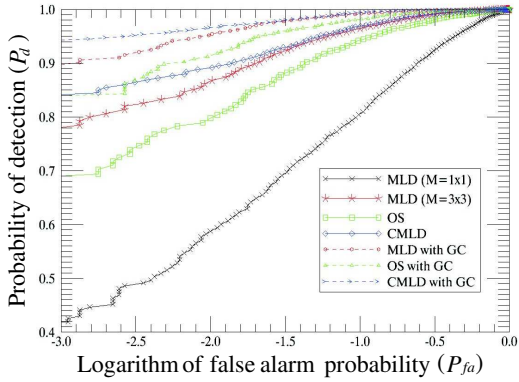

Figure 9. Experimental ROC curves corresponding to the acquisitions of January 01 and January 09, 2009. $M = 3 \times 3$, $n_{os} = 5$ and $k = 5$.

6. CONCLUSION

In the present paper, we consider the use of COSMO-SkyMed SAR images for Coherent Change Detection. Three detectors (Mean Level Detector, Ordered Statistic and Censored Mean Level Detector) are applied to coherence image in order to detect surface changes. The probabilities of detection and false alarm are evaluated experimentally using CSK images. The results show that CMLD is well suited to this kind of problem. We also propose to incorporate guard cells and particularly when using SAR data, due to the high correlation coefficient in range direction versus azimuth direction. It is shown that the proposed method, CMLD with guard cells only in the range direction, is robust and provides almost 4% higher detection probability in the case of low probability of false alarm.

ACKNOWLEDGMENT

The authors would like to express their gratitude to D. Borghys (RMA Belgium) and N. Hannoun (USTHB Algeria) for their helpful comments. The SAR data was obtained through a collaboration within NATO SET145 and processed in the Belgian Royal Military Academy. We thank the private companies Sarmap and ITTVis for their support in providing a full Sarscape licence (v. 4.8, 2011) included in the latest version of Envi software. Comments and suggestions formulated by the anonymous reviewers were very helpful in completing the revised manuscript.

REFERENCES

1. Just, D., "Phase statistics of interferograms with applications to synthetic aperture radar," *Appl. Opt.*, Vol. 33, No. 20, 4361–4368, 1994.
2. Rignot, E. J., "Change detection techniques for ERS-1 SAR data," *IEEE Trans. Geosci. Remote Sens.*, Vol. 31, No. 4, 896–906, 1993.
3. Preiss, M., "A change detection statistic for repeat pass inteferometric SAR," *Proc. ICASSP*, 938–940, 2003.
4. Zebker, H. A., "Decorrelation in interferometric radar echoes," *IEEE Trans. Geosci. Remote Sens.*, Vol. 30, No. 5, 950–959, 1992.
5. Touzi, R., "Coherence estimation for SAR imagery," *IEEE Trans. Geosci. Remote Sens.*, Vol. 37, No. 1, 135–149, 1999.
6. Preiss, M., "Scene coherency at X-band from repeat pass polarimetric interferometry," *Proc. IEEE Int. Geosci. Remote Sens. Symp.*, 1081–1084, 2005.
7. Oishi, N., "A coherence improvement technique for coherent change detection in SAR interferometry," *Proc. of the 6th European Radar Conference*, Rome, Italy, September 30–October 2, 2009.
8. Sabry, R., "A new coherency formalism for change detection and phenomenology in SAR imagery: A field approach," *IEEE Geosc. and Remote Sens. Letters*, Vol. 6, No. 3, 458–462, 2009.
9. Hochino, T., "Coherent change detection with complex logarithm transformation on SAR imagery," *SICE Annual Conference*, Taipei, Taiwan, August 18–21, 2010.
10. Papathanassiou, K. P., "Single-baseline polarimetric SAR interferometry," *IEEE Trans. Geosci. Remote Sens.*, Vol. 39, No. 11, 2352–2363, 2001.
11. Gatelli, F., "The wavenumber shift in interferometry," *IEEE Trans. Geosci. Remote Sens.*, Vol. 32, No. 4, 855–865, 1994.
12. Hanssen, R. F., *Radar Interferometry, Data Interpretation and Error Analysis*, Kluwer Academic Publishers, 2002.
13. Rohling, H., "Radar CFAR thresholding in clutter and multiple target situations," *IEEE Trans. on Aeros. and Elect. Syst.*, Vol. 19, No. 4, 608–621, 1983.
14. Rickard, J. T., "Adaptive detection algorithms for multiple target situations," *IEEE Trans. on Aeros. and Electr. Syst.*, Vol. 13, No. 10, 338–343, 1977.